RSC Advances

ROYAL SOCIETY OF CHEMISTRY

www.rsc.org/advances

Journal Name

RSCPublishing

ARTICLE

Performance of the hydroxyapatite coatings electrodeposited on micro-arc oxidized magnesium alloys using static magnetic field

Cite this: DOI: 10.1039/x0xx00000x

Received 00th January 2012,
Accepted 00th January 2012

DOI: 10.1039/x0xx00000x

www.rsc.org/

Quan Xu[a*], Yao Liu[a], Chuangwei Liu[b*], Ang Tian[c], Xiaoguo Shi[c], Chenbo Dong [d], Ying Zhou[a], Hongjun Zhou[a]

Biodegradable magnesium (Mg) and its alloy is one of the most widely used functional materials for the osteosynthetic application due to their rapidly degradation property and requiring no surgical removal. However, the rapid degradation of magnesium alloy could cause the high alloy corrosion rate, which need to be regulated during bone healing process. In this work, we coated hydroxyapatite (HA) crystal nanostructure on magnesium alloy to inhibit the corrosion via the electrodeposited process in the presence of static magnetic field. The physical and chemical properties of HA coatings were characterized using SEM, XRD, EDS, as well as corrosion test. In addition, how interaction between such coated and osteoblast cell regulated cellular behavior was investigated. The result indicted that the corrosion resistance ability of the magnesium alloy coated with HA was improved significantly compared with uncoated magnesium alloy. The initial corrosion potential of Ca-P composite coating at -0.5V was achieved, which was almost one third of the potential value of the pure magnesium alloy (AZ91D). The proliferation, adhesion and expression analysis of IGF-1 protein indicated that the HA nanocrystal could enhance the viability of the cells. This work provided insight to develop next generation of biocompatible alloy for biomedical application.

1. INTRODUCTION

Magnesium-based implants attracted more and more attention in biological and biomedical field especially for orthopedic application because of the excellent biocompatibility and biodegradable properties.[1] Compared with the titanium-based implants which was also currently used clinically, magnesium possessed significantly higher bone-implant contact and superior osseointegration,[2] which would improve the biological fixation and anchorage in host bone. However, the low corrosion resistance of magnesium would lead to the loss of mechanical integrity[3] as well as the disharmony between the kinetics of degradation and bone healing.[4] To overcome the intrinsic drawback of the magnesium, various studies aiming to maintain magnesium strength has been carried out,[3] and the interaction between corrosion of alloy and association of bone response has been also investigated intensively.[5,6] Among various methods, the magnesium modified by element alloying has exhibited the potential advantage for their contacting with surrounding bone directly during the degradation,[5] which retarded mechanical properties loss, and the relevant mechanisms were also revealed.[7] This hard alloy functional materials are differed from traditional soft polymer based biomaterials,[8-13] due to their nanoscale structure character, mechanical property, large surface area and unique porous nature, as well as their novel chemical physical properties, i.e. electrochemical properties, which are not usually seen in organic molecular based polymer materials. In addition, with chemical surface modification, alloy functional materials could achieve mimic extracellular matrix (ECM)[14] function to regulate cellular behavior via controlling interaction at cell-substrate interface. Specially, such magnesium alloy displayed light density,[15] high Young's modulus which is similar with natural bone,[1, 16] as well as low health risk and adverse effect on biological system, therefore gained widely attention in bone implant field. For example, Kraus et al. investigate degrading magnesium pin implants in the growing rat skeleton, it

was found that such magnesium displayed good osteoconductive properties by enhancing bone accumulation at the pin surface.[17] Dziuba et al. developed magnesium alloy ZEK100 to improve stability of such resorbable materials for osteosynthesis. It exhibited very high initial stability and excellent biocompatibility in the animal model over 9 and 12 months.[18] On the other hand, pre-treated surface of magnesium alloy was also an promising strategy for overcoming the drawbacks of high corrosion rate.[19],[20] Previous studies suggested that the magnesium-based metal-inorganic matrix materials would further improve the performance of implants in terms of the bioactive and corrosion behavior compared with magnesium and titanium alloy.[21, 22] The debate on the element alloying also indicate that the impurities and secondary phases would generate the internal galvanic corrosion and cause the adverse effects.[23] In addition, the alternation of pH caused by the liberation of hydrogen would impact the bone reconstruction.[24] Among varies type of magnesium alloy surface functional coating technologies, layer-by-layer deposition exhibited distinguished biocompatibility and would inhibit the gas generation.[22] Particularly, the HA/MAO composite coatings have been used as an intriguing treatment for improving the corrosion resistance and cellular integration.[25-26] Micro-arc oxidation (MAO), a plasma-electrolytic oxidation technology, could remarkably enhance corrosion resistance of magnesium alloy in various condition via creating barrier on the surface of the metal,[25-27] and such MAO modified magnesium alloy have been widely used in biomedical and tissue engineering field.[28] Hydroxyapatite (HA) was the most widely used bioactive inorganic biomaterials. For example, it has been used for the osseointegration and fracture healing in the clinic for decades.[29] However, the relative low stiffness limit its application in some content. In the structure of the HA/MAO, the porous MAO coatings would serve as adequate support for implantation of HA particles (micro or nano size) to enhance its mechanics for biomedical utilization. Although the mechanism associated to the corrosion behavior and biocompatibility of HA/MAO coatings have been discussed by amount of previous studies, the precise control of the phase and topography of the HA coatings were still not fully achieved.[20] In addition, the topography and phase of materials could regulate cellular behavior, thus to obtain user-controlled coating with specific properties is necessary.

In our study, AZ91 (magnesium alloy containing Al and Zn elements) was employed as the substrate for supporting the HA/MAO composite coatings. Because of the excellent mechanical property and corrosion resistance, AZ91 has been widely used as the implant material in the academia researches and clinical applications.[5, 30] The magnesium without coated HA/MAO was regards as control sample, and the functional coatings were fabricated by the MAO/EPD method.[31] In addition, the topography of the HA coatings was modified by the magnetic field, which has been demonstrated as the effective method to regulate the size of the HA particles.[31] The coating performances such as the topography, corrosion resistance and transformation of phase were evaluated. The interaction between the biocompatibility and coatings performance was also analyzed using MTT and osteoblast staining testing, and the relevant mechanism was discussed.

2. EXPERIMENTAL

2.1 Fabrication of HA/MAO coatings

Die-cast AZ91D magnesium alloy (Al 9.22 wt.%, Zn 0.72 wt.%, Mn 0.418 wt.% and Mg balance) was cut into disc shape with 2×2 cm^2, pretreated by the ground of SiC papers (200 grits, 600 grits, 1200 grits, respectively), and the alloy was sonicated in acetone, then dried in N_2 atmosphere for the subsequent anodization. Mageniusm alloy after treatment was selected as working electrodes and Pt electrodes were selected as counter electrodes. the MAO film was fabricated in 10 g/l $Na_2SiO_3 \cdot 9H_2O$, 5 g/l $Na_3PO_4 \cdot 12H_2O$, 2 g/l NaOH and 1.5 g/l CaF_2 solution under pulse voltage mode with 300-400 V for 20-30 min under temperature (20-30 ℃). After the anodization process, the samples were ultrasonically rinsed with acetone and distilled water, respectively, and then dried in air for the electro deposition.

Uniform HA coating was formed by electrochemically deposition on MAO film under the static magnetic fields. The electrolyte contained 0.1 mol/L calcium nitrate ($Ca(NO_3)_2$), 0.04 mol/L sodium nitrate ($NaNO_3$) and 0.06 mol/L ammonium dihydrogen phosphate ($NH_4H_2PO_4$), where the MAO film was served as cathode and the platinum was served as counter electrode. The pH of electrolyte was adjusted to 6 using the nitric acid and the electrochemical deposition was achieved at 85 ℃ with current density of 10 mA/cm^2 for 60 min. The teflon electrochemical bath was placed in the static magnetic filed, and the direction of the magnetic in this study was parallel to the electric field (B=1 T). The magnesium coated with the HA/MAO without magnetic was also used as control.

2.2 Characterization and Test

Immersion tests were carried out in Hank's solution （8 g/l NaCl, 0.4 g/l KCl, 0.25 g/l $NaH_2PO_4·H_2O$, 0.35 g/l $NaHCO_3$, 0.06 g/l $Na_2HPO_4·2H_2O$, 0.19 g/l $MgCl_2$, 0.19 g/l $CaCl_2·2H_2O$, 0.06 g/l $MgSO_4·7H_2O$ and 1 g/l glucose, pH 7.8）at 37±0.5 ℃ according to ASTM-G31-72. Specially, samples were removed after 7 days immersion, rinsed with distilled water (Di water) and dried in air. The surface morphology of composite coating was characterized using scanning electron microscope (SEM, S-4800, Hitachi, Japan) with working condition at 15 KV. The crystalline structure of sample was analyzed by X-ray diffraction (XRD, D8211, Huber, Netherlands) with Cu Kα radiation source, and the chemical compositions of samples were examined by energy dispersive spectroscopy (EDS, EX, Horbia, Japan). Electrochemical measurements were performed using a three electrode system to determine corrosion resistance ability of samples. Saturated calomel electrode (SCE) and platinum sheet were used as the reference and counter electrodes, respectively. Potentiodynamic polarization curves were measured at a scan rate of 1 mV/s by using an electrochemical workstation (CHI 650C, China). The bond of the Ca-P coatings and the alloy was investigated by the adhesive strength test.[32]

2.3 Cell culture

Human osteoblasts (bone-forming cells) were purchased from American Type Culture Collection (CRL-11372).Specially, human osteoblast (HOB) cell Human osteoblasts were cultured in Dulbecco's Modified Eagle Medium (DMEM) containing 10% fetal bovine serum(FBS), 1% penicillin, and 1% streptomycin in at 37℃ with 5% CO_2 humidified atmosphere environment. The culture medium was replaced every other day and passaging the cells was subcultured through trypsinization when they reach to 80% confluence. All samples (Nine examples for each type of implant) were sterilized by ethylene oxide, then placed in plastic petri dishes with 24 wells. Human osteoblasts were seeded onto Ti, NT and NT/Vancomycin (all substrates were 2 cm×2 cm) with initial density of 10^4 cells/cm^2.

2.4 Cells proliferation and adhesion analysis

The osteoblast adhesion was investigated after 6 , 24 , 48 h and the cell viability was determined using MTT assay. Human osteoblast cells were cultured onto bare Ti, TNT, TNT/vancomycin substrates at an initial density of 1×10^4 cells /cm^2, respectively. After 6, 12, 24 h, the samples were washed by PBS buffer and transferred to a new 12-well cell culture plate for analysis. The samples were changed with 500 μl of fresh culture medium and 0.1 ml of MTT solution. The cells were incubated at 37℃ for additional 4 h. Then, MTT contained medium was removed and 500 μl of dimethyl sulfoxide was added to each well to dissolve all the generated formazan dyes. The optical density of the solution was measured at a wavelength of 570 nm. Human osteoblast cell viability was calculated by the equation: mean OD/blank control mean OD × 100. All MTT assays were repeated for three independent experiments, each experiment contained at least six replicates.

2.5 Cell viability (AO/EB) analysis

Cell viability was determined by acridine orange/ethidium bromide (AO/EB) assay. The osteoblasts were cultured onto the bare Ti, NT, and NT-V substrates with an initial density of 2×10^4 cells/cm^2. After 12 and 24 h, the samples were washed in PBS buffer. The living and dead cells were stained with AO/EB at room temperature and observed on the CLSM (confocal laser-scanning microscope).

2.6 Immunofluorescence analysis of osteogenesis-related proteins

After 7 days, the cells cultured on the nHA/MAO, μHA/MAO and uncoated magnesium alloy were fixed in 4% paraformaldehyde in 1×PBS buffer for 30 min at room temperature. After washing three times with PBS (5 min for each time), cells were permeabilized in 1% Triton X-100 in PBS for 5 min. Then cells were washed twice with PBS (5 min for each time), followed by incubated with 1% BSA/1×PBS at room temperature. The cells was incubated for 12 h with addition of primary antibody (1: 200)(Gibico, USA) and anti-IGF-1. After washed for three times with 0.1M PBS (5 min for each time), the sections were incubated with the secondary antibody (Gibico, USA)(1: 200) for 1 h at 37 °. The HOB cell was stained with DAPI at room temperature, and then observed on confocal laser scanning microscope for immunofluorescence analysis.

2.7 Statistical analysis

Statistical analysis was performed using a student's test using SPSS software. The transition of the number of bacteria between each metal and MTT assay (by OD) were analyzed by variance (ANOVA) test. The data is expressed as mean ± standard deviation, Statistical significance was considered at $P < 0.05$.

3. RESULTS AND DISCUSSION

3.1 Morphology of the HA/MAO coatings

The morphologies of three samples were shown in Fig. 1a, the surface of the magnesium was smoothly, and the trace caused by the ground treatment could be obviously observed; the HA/MAO coatings fabricated by the electrodeposition with or without presence of magnetic field exhibited different topography as Fig. 1b and c illustrated. The HA particles in the composite coatings were spherical with the diameter about 30-50 nm, it is interesting to note that the morphology of the coating dramatically changed, exhibiting broccoli-like shape with less than 5 μm diameters. The transformation of the topography of HA coatings was consistence with our previous studies, specially, the spherical nanoparticles were formed in the presence of the magnetic field.[31] The XRD results indicated that the formation of MgO passivated in the air, and each elements of was distributed in the alloys.(Fig. 1d) The characteristic HA peaks could be observed in the XRD curves of HA/MAO coatings with or without presence of magnetic field, in addition, the nano-size effect and the amorphous phase lead to the broaden peak in the nHA/MAO coatings. For supporting the HA coatings, MAO coatings was introduced to enhance the binding between the HA coating and alloy substrate. The cross section morphologies of MAO layer were investigated by SEM, and the thickness of MAO layer is about 8 μm.(Fig. 1c) . It was observed that the Ca-P ceramic coated structures micro-arc oxidized magnesium alloys displayed high porosity structures and calderas appeared in the layers. The molten oxide particles caused by the sintering process were randomly distributed and formed large aggregations, pores could be formed on the molten oxide and gas bubbles were thrown out of micro-arc discharge channels.[33] In addition, the peaks shown in the curve corresponded with crystal plan of Mg_2Ca, Ca_3SiO_5 and $Ca(PO_3)_2$ (Fig. 1c), respectively, confirm the existence of the composite phase besides the main MgO phase. The presence of Mg_2Ca, Ca_3SiO_5 and $Ca(PO_3)_2$ indicated the participation of the elements (Si, Ca and P) in the electrolyte during the chemical reactions.[25] What's more, the EDS results (as shown in Fig. 1c) further confirm the presence of abundant elements mentioned above. Therefore, the calcium phosphate ceramic layer could provide the favourable gradient

coating to electrodeposit Ca-P biological film in for further experiment.

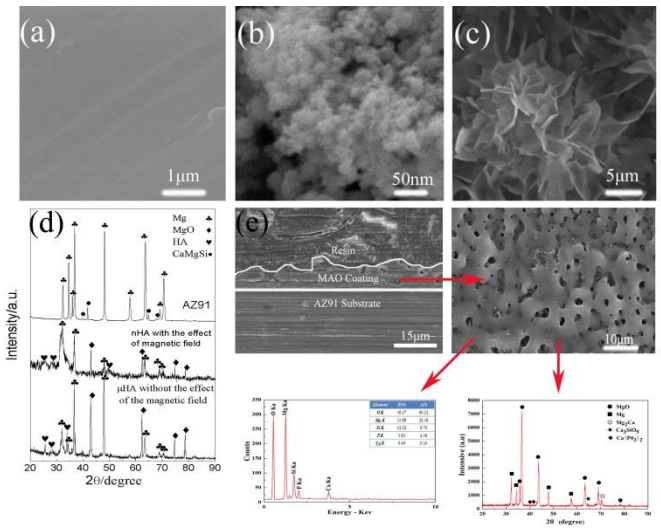

Fig. 1. (a): smooth magnesium surface; (b): spherical nHA particles deposited on the MAO coatings with the synergy effect of magnetic field; (c): μHA crystals deposited on the MAO coatings without the synergy effect of magnetic field; (d): the XRD pattern of AZ91 surface, nHA/MAO coatings and μHA/MAO coatings ; (e): the surface and cross-section morphology of the MAO coatings, the XRD and EDS of the MAO coatings.

3.2 Performance of the HA/MAO in the SBF

The morphology, phase transformation and the passivation potential of the samples was investigated. In the immersion test, it was found the coatings with significant structure change could be observed in three samples after 1 week immersion. For the nHA/MAO, after immersion in SBF for 1 week, the nHA crystal transform into the flake crystals, and the coatings were tightly and neatly as Fig 2a showed; for the μHA/MAO coatings, after 1 week immersion, the HA crystals accumulated into compact cakes and the coatings were looser than the nHA coatings. However, the magnesium alloy was coated by the flocculence sediments and the fractions could be observed significantly. In this study, for the nHA/MAO and μHA/MAO, the HA crystals generation and formation during the calcification process was considered as a nucleation template in SBF incubation, offering hydroxyl terminals known as efficient inducers of apatite nucleation.[34] These hydroxyl terminals would enroll Ca^{2+} in the SBF firstly, followed by Cl^{-}, $H_2PO_4^{-}$ and CO_3^{2-}. The same crystal structure to apatite and the rough porous morphologies of the HA obtained during the calcification may also promote apatite nucleation. Some reports demonstrated that most negatively charged groups strongly induced apatite formation.[34] In addition, the pH value of solution would elevate corresponding with substrate degraded in SBF, and then the Ca^{2+} and phosphate ions (such as PO_4^{3-} and HPO_4^{2-}) in the solution would react with each other to form abundant Ca-P salt precipitating on the sample. On the other hand, the Ca-P coatings formed on the magnesium alloy might go through different transformation of the HA crystal compared with the HA/MAO coatings. The formation of Ca-P group was the first step during the initial immersion period, and the component ions or groups would be absorbed onto the Ca-P group, the DCP would formed subsequently as the XRD and EDS analysis confirmed in Fig2. Specially, due to the deposition of the Ca-P coatings was modulated by the settlement action, the bind force between the coatings and the substrate was lower than that of the HA/MAO coatings, thus, the fraction would be observed.

To further investigate Ca-P coating corrosion resistance ability, potentiodynamic polarization test was performed. Fig. 2e shows potentiodynamic polarization curves of untreated magnesium alloy and 2 types of HA/MAO layers in SBF. It is worth to note that the corrosion potential of 2 types of Ca-P/MAO layers were about -0.5 V (vs. SCE) and -0.75 V, respectively, positive than that of magnesium alloy (-1.37 V(vs. SCE)). The slope of the curve of untreated magnesium alloy sample increased fast at the beginning of the anodic side and then diffusion-controlled anodic current was observed at the end of the curves due to the fast corrosion rate. It is indicated that untreated magnesium alloy substrate suffered severe erosion in SBF comparing with Ca-P coating. The Ca-P coating has better performance on corrosion resistant for sealing layer effect, and the compact coatings would improve the corrosion resistance which was confirmed by the performance of the nHA/MAO coatings

immersed for 1 week. The different polarization behaviors of the Ca-P coating and the magnesium alloy can be attributed to their different properties and structures. The MAO layer has relatively high porosity and calderas on the surface as observed in Fig. 1e. Therefore, by increasing anodic potential during polarization, corrosive intermediate (Cl^-) would be rapidly transferred through the outer porous layer and reached the inner barrier layer of the MAO, resulted in the increase of polarization current. When the polarization current reaches a certain value, the corrosive intermediate would react with the MAO layer and produce pits on the layer. For the Ca-P coating species, the transfer of corrosive intermediate (Cl^-) was inhibited in certain extent and the increase of polarization current was suppressed during polarization process, due to the covering and blocking effect of the sealing layer. As a result, the corrosion process of the composite coating was delayed.

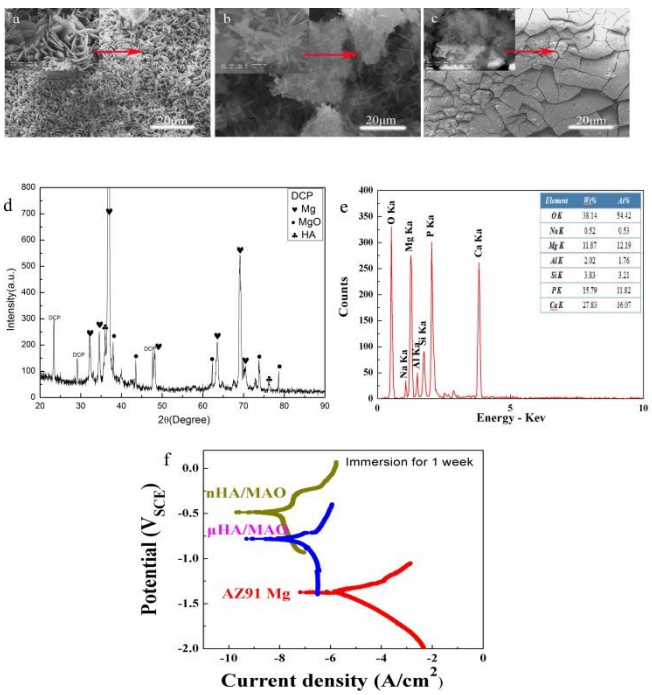

Fig. 2. (a-c): morphology of the nHA/MAO coatings, μHA/MAO coatings and magnesium surface immersed for 1 week immersed for 1 week; (d): XRD pattern of the coatings formed on the AZ91 substrate immersed for 1 week; (e): EDS of the coatings formed on the AZ91 substrate immersed for 1 week; (f): polarization curves of nHA/MAO coatings, μHA/MAO coatings and AZ91 substrate immersed for 1 week in SBF.

3.3 Cytocompatibility of the HA/MAO coatings

Osteoblast is widely used cell line model in orthopaedics research.[35] Specially, osteoblast has been employed to evaluate various alloy components potential application for bone implant. Tiainen et al investigated biological response of osteoblast cells to carbon-coated TiO_2. It was observed in this study that carbon coating could promote ALP activity and osteogenic protein gene expression (PCR), as well as enhance osteoblast proliferation.[36] In our work, the adhesion and proliferation analysis of osteoblast was employed to evaluate the cytocompatibility of the HA/MAO coatings. The MTT assay is a colorimetric assay for evaluating the mitochondrial dehydrogenase activity in cell. In the presence of NAD(P)H-dependent cellular oxidoreductase enzymes, MTT (a yellow tetrazole) could be reduced to its its insoluble formazan, which has a purple color. Solution of dimethyl sulfoxide is added to dissolve the insoluble purple formazan product into a colored solution. The absorbance of such colored solution can be quantified by measuring at a certain wavelength to determine the mitochondria activity, which reflects the cell activity. After 24 h culture, the nHA/MAO coatings could enhance the cell adhesion significantly compared with the μHA/MAO and uncoated magnesium alloy. Up to 72 h, the enhancement observed was even obvious. Correspondingly, the MTT results further indicated that the nanostructure crystal HA coatings would improve the activity of the cells considerably (Fig. 3b). In addition, the AO/EB staining demonstrated that all the samples would inhibit the apoptosis of the cells. Specially, the amount of the osteoblasts cultured on the nHA/MAO coatings was the highest, then are the cells cultured on micro HA/MAO coatings, the number of the cells cultured on the magnesium was the lowest. In addition, to further investigate the consequences for increased cell adhesion and proliferation on nHA/MAO coatings, we sought to examine the expression of the proliferation-related protein, insulin-like growth factor-1 (IGF-1), by the Immunofluorescence analysis. The IGF-1 was the mitogenic factor, which would be used to stimulate osteoblast growth and proliferation, and the high

expression of the IGF-1 would lead to the enhanced osseointegration.[37]

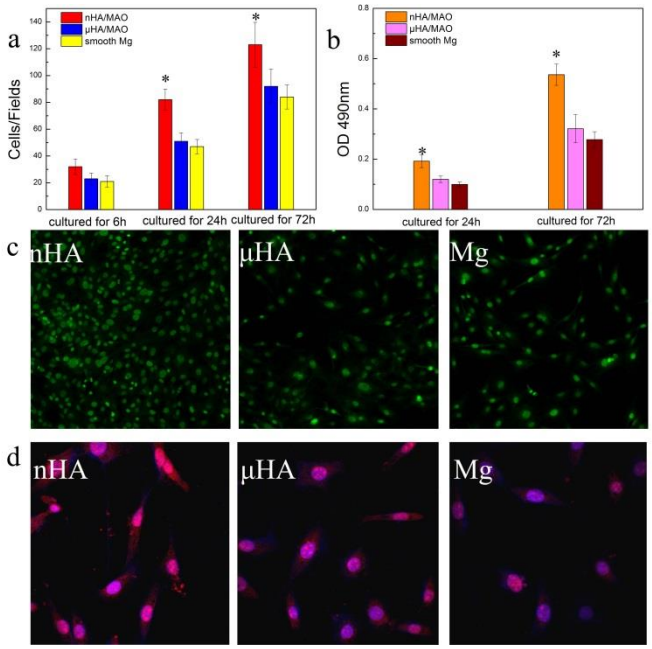

Fig. 3. Behaviors of the osteoblast (CRL-11372) on different coatings: (a): adhesion of cells on nHA/MAO coatings was increased compared with μHA/MAO coatings and magnesium alloy after cultured for 24h(*$P<0.05$, compared to μHA/MAO coatings and magnesium alloy) ; (b): the proliferation of the cells cultured on the nHA/MAO coatings was higher than that of μHA/MAO coatings and magnesium alloy after cultured for 24 h(*$P<0.05$, compared to μHA/MAO coatings and magnesium alloy); (c): Fluorescence micrographs of the osteoblast cells cultured for 24 h on nHA/MAO coatings, μHA/MAO coatings and magnesium alloy. Living cells (green) and dead cells (red) were stained with acridine orange/ethidium bromide and were visualized using fluorescence microscopy; (d): Staining of IGF-1 of cells cultured on three samples

The expressions of the IGF-1 (Fig. 3d) indicated that the enhanced viability and activity of the cells could be attributed to the higher expression of growth factor in cells cultured on the nHA/MAO coatings. The HA coatings could offer the osteoblast a close native environment, therefore the osteoblast exhibited increased proliferation and viability on the HA/MAO coatings compared with the smooth magnesium substrate.[38] The HA with nanostructure displayed significance advantage on the osseointegration compared with the micro scale HA crystal. Due to the nano-size structure,.the phase of the nHA was amorphous (the broaden peak as Fig. 1b showed), and the dissolution rate was higher than the micro-HA particles,[39] thus the nHA coatings would lead to the high extracellular Ca^{2+} concentration, and the high Ca^{2+} concentration would enhance the proliferation and viability of the cells by up-regulating the expressions of the proteins related to the bone genes such as the IGF-1, osteopontin, osteocalcin and bone sialoprotein.[40] Although the nHA particles exposing to the cells (especially the monocytes or macrophages) would result in the death of the cells,[41] the mode of interaction between nanoparticles and cells would be responsible for the different fates of cells after treated by the nHA particles. The cells cultured with the gel of nHA particles (especially the small spherical HA nanoparticles) would result in the particles uptake in cells,[41] subsequently, nHA particles would dissolve under the effect of the lysosome and release Ca^{2+} into the cytoplasm, the intracellular Ca^{2+} homeostasis would be broken by the increased Ca^{2+} ions which was the main cause of the cytotoxicity.[39] In our study, the cells were cultured on the nHA coatings which were constituted by the large agglomeration of HA nanocrystals, the nHA particles were not dispersal in the medium and the state of the nHA agglomeration confine the cytophagy (only the size of agglomeration with smaller than 500 nm could be swallowed by cell). On the other hand, the concentration of the nHA gel, the preparation as well as the chemical characteristics of the particles would influence the toxicity of the nHA particles, the suspended gel preparation with more than 31 μg/ml would be toxic, other preparations were also toxic but only at higher than 250 μg/ml. The results of our study indicated that the nHA coatings would promote the proliferation of osteoblast, which was caused by the increased extracellular Ca^{2+} concentration as well as the regulation of the signaling pathway triggered by Ca^{2+}. The small amount nHA particles uptake by the cells might contribute invalid effect on the cells behaviors. In addition, the geometry and scale of nanocoating also should be responsible for the increased adhesion of cells. Previous report indicated that the nanotopography and the

nanopattern coatings (i.e. the nanotubes and the nanospherical paticles) could up-regulate the activity of the integrin and adhesive protein.[42] Thus, it's reasonable to assume that the significant distinguish of viability of cells cultured on different coatings also could be attributed to the nanostructure dimensional effect.

4. Conclusions

A calcium phosphate coating was successfully generated on the micro-arc oxidized magnesium surface using electrodeposition method. With the synergy effect of the static magnetic field, the spherical HA crystal with nanostructure was achieved. After soaking in SBF, the morphologies of calcification coating have changed dramatically in the different coatings. The nHA coating exhibited excellent corrosion resistance in SBF because of (give the reason). The proliferation and viability of the cells could be improved when cultured on the nHA/MAO coatings due to the high expression level of the IGF-1. Our work provide insight for developing novel clinic orient biocompatible functional materials.

Acknowledgements

We thank Science Foundation of China University of Petroleum Beijing (No. 2462014YJRC011) and the National Natural Science Foundation of China (No. 50872018, 51002027), scientific foundation of educational department of Liaoning Province (L2012084) and Project of Ministry of education of basic scientific research (N130402001) for the support.

Notes and references

[a] Institute of New Energy, State Key Laboratory of Heavy Oil Processing, China University of Petroleum (Beijing), Beijing, 102249, China.
[b] Mechanical Engineering Department, University of North Texas, Denton TX, 76207, USA.
[c] School of Materials and Metallurgy, Northeastern University, Shenyang, 110819, China.
[d] Department of Civil and Environmental Engineering, Rice University, Houston, Texas 77005, United States.
* Corresponding author:
xuquan@cup.edu.cn, liucw007@gmail.com

1. M. P. Staiger, A. M. Pietak, J. Huadmai and G. Dias,*Biomaterials*, 2006, **27**, 1728-1734.
2. C. Castellani, R. A. Lindtner, P. Hausbrandt, E. Tschegg, S. E. Stanzl-Tschegg, G. Zanoni, S. Beck and A.-M. Weinberg, *Acta Biomater.*, 2011, **7**, 432-440.
3. Y. Chen, Z. Xu, C. Smith and J. Sankar, *Acta Biomater.*, 2014, **10**, 4561-4573.
4. S. V. Dorozhkin, *Acta Biomater.*, 2014, **10**, 2919-2934.
5. F. Witte, V. Kaese, H. Haferkamp, E. Switzer, A. Meyer-Lindenberg, C. J. Wirth and H. Windhagen, *Biomaterials*, 2005, **26**, 3557-3563.
6. N. T. Kirkland, N. Birbilis and M. P. Staiger, *Acta Biomater.*, 2012, **8**, 925-936.
7. Y. Xin, T. Hu and P. K. Chu, *Acta Biomater.*, 2011, **7**, 1452-1459.
8. X. A. Gong, L. L. Han, Y. A. Yue, J. R. Gao and C. Y. Gao, *J. Colloid. Interf. Sci.*, 2011, **355**, 368-373.
9. X. Gong, L. L. Han, J. R. Gao and C. Y. Gao, *Colloids Surf., A*, 2012, 396, 299-304.
10. X. Gong, *RSC Adv.*, 2014, **4**, 54494-54499.
11. X. Gong and C. Y. Gao, *Phys. Chem. Chem. Phys.*, 2009, **11**, 11577-11586.
12. C. N. Kotanen, A. N. Wilson, C. B. Dong, C. Z. Dinu, G. A. Justin and A. Guiseppi-Elie, *Biomaterials*, 2013, **34**, 6318-6327.
13. A. Guiseppi-Elie, C. B. Dong and C. Z. Dinu, *J. Mater. Chem.*, 2012, **22**, 19529-19539.
14. J. T. Li, K. C. Hansen, Y. Zhang, C. B. Dong, C. Z. Dinu, M. Dzieciatkowska and M. Pei, *Biomaterials*, 2014, **35**, 642-653.
15. B. L. Mordike and T. Ebert, *Mater. Sci. Eng.*, 2001, **302**, 37-45.
16. R. C. Zeng, W. Dietzel, F. Witte, N. Hort and C. Blawert, *Adv. Eng. Mater.*, 2008, **10**, B3-B14.
17. T. Kraus, S. F. Fischerauer, A. C. Hanzi, P. J. Uggowitzer, J. F. Loffler and A. M. Weinberg, *Acta Biomater.*, 2012, **8**,1230-1238.
18. D. Dziuba, A. Meyer-Lindenberg, J. M. Seitz, H. Waizy, N. Angrisani and J. Reifenrath, *Acta Biomater.*, 2013, **9**, 8548-8560.
19. W. Cui, E. Beniash, E. Gawalt, Z. Xu and C. Sfeir, *Acta Biomater.*, 2013, **9**, 8650-8659.
20. H. Hornberger, S. Virtanen and A. R. Boccaccini, *Acta*

Biomater., 2012, **8**, 2442-2455.

21. Q. Xu, P. Pu, J. Zhao, C. Dong, C. Gao, Y. Chen, J. Chen, Y. Liu and H Zhou, *J. Mater. Chem. A*, 2015, **3**, 542-546
22. N. Ostrowski, B. Lee, N. Enick, B. Carlson, S. Kunjukunju, A. Roy and P. N. Kumta, *Acta Biomater.*, 2013, **9**, 8704-8713.
23. G. Song, A. Atrens, X. Wu and B. Zhang, *Corros. Sci.*, 1998, **40**, 1769-1791.
24. R. Rojaee, M. Fathi and K. Raeissi, *Mat. Sci. Eng. C-Mater.*, 2013, **33**, 3817-3825.
25. F. Chen, H. Zhou, B. Yao, Z. Qin and Q. Zhang, *Surf. Coat. Tech.*, 2007, **201**, 4905-4908.
26. H. Duan, K. Du, C. Yan and F. Wang, *Electrochim. Acta*, 2006, **51**, 2898-2908.
27. W. Shang, B. Chen, X. Shi, Y. Chen and X. Xiao, *J. Alloy. Compd.*, 2009, **474**, 541-545.
28. S. M. Reshetnikov, E. V. Kharanzhevskii and M. D. Krivilev, *Prot. Met. Phys. Chem.*, 2012, **48**, 729-734.
29. K. M. Hennessy, W. C. Clem, M. C. Phipps, A. A. Sawyer, F. M. Shaikh and S. L. Bellis, *Biomaterials*, 2008, **29**, 3075-3083.
30. R. Rojaee, M. Fathi and K. Raeissi, *Mat. Sci. Eng. C-Mater.*, 2013, **33**, 3817-3825.
31. C. Liu, A. Tian, H. Yang, Q. Xu and X. X. Xue, *Appl. Surf. Sci.* 2013, **287**, 218-222.
32. X. Shi, A. Tian, X. Xue, H Yang, and Q. Xu, *Mater. Lett.*,2015, **141**, 104-106.
33. H. F. Guo and M. Z. An, *Appl.Surf.Sci., 20*05, **246**, 229-238.
34. G. K. Toworfe, R. J. Composto, I. M. Shapiro and P. Ducheyne, *Biomaterials*, 2006, **27**, 631-642.
35. V. Kartsogiannis and K. W. Ng, *Mol. Cell Endocrinol.*, 2004, **228**, 79-102.
36. K. S. Brammer, C. Choi, C. J. Frandsen, S. Oh, G. Johnston and S. Jin, *Acta Biomater.*, 2011, **7**, 2697-2703.
37. S. Kim, Y. Q. Kang, C. A. Krueger, M. L. Sen, J. B. Holcomb, D. Chen, J. C. Wenke and Y. Z. Yang, *Acta Biomater.*, 2012,**8** 1768-1777.
38. M. J. Dalby, L. Di Silvio, E. J. Harper and W. Bonfield, *Biomaterials*, 2002, **23**, 569-576.
39. M. Motskin, D. M. Wright, K. Muller, N. Kyle, T. G. Gard, A. E. Porter and J. N. Skepper, *Biomaterials*, 2009, **30**, 3307-3317.
40. A. M. C. Barradas, H. A. M. Fernandes, N. Groen, Y. C. Chai, J. Schrooten, J. van de Peppel, J. P. T. M. van Leeuwen, C. A. van Blitterswijk and J. de Boer, *Biomaterials*, 2012, **33**, 3205-3215.
41. J. L. Xu, K. A. Khor, J. J. Sui, J. H. Zhang and W. N. Chen, *Biomaterials*, 2009, **30**, 5385-5391.
42. G. Mendonca, D. B. S. Mendonca, F. J. L. Aragao and L. F. Cooper, *Biomaterials*, 2008, **29**, 3822-3835.

Figure Captions

Fig. 1. (a): smooth magnesium surface; (b): spherical nHA particles deposited on the MAO coatings with the synergy effect of magnetic field; (c): μHA crystals deposited on the MAO coatings without the synergy effect of magnetic field; (d): the XRD pattern of AZ91 surface, nHA/MAO coatings and μHA/MAO coatings ; (e): the surface and cross-section morphology of the MAO coatings, the XRD and EDS of the MAO coatings.

Fig. 2. (a-c): morphology of the nHA/MAO coatings, μHA/MAO coatings and magnesium surface immersed for 1 week immersed for 1 week; (d): XRD pattern of the coatings formed on the AZ91 substrate immersed for 1 week; (e): EDS of the coatings formed on the AZ91 substrate immersed for 1 week; (f): polarization curves of nHA/MAO coatings, μHA/MAO coatings and AZ91 substrate immersed for 1 week in SBF.

Fig. 3. Behaviors of the osteoblast (CRL-11372) on different coatings: (a): adhesion of cells on nHA/MAO coatings was increased compared with μHA/MAO coatings and magnesium alloy after cultured for 24h(*$P < 0.05$,compared to μHA/MAO coatings and magnesium alloy) ; (b): the proliferation of the cells

cultured on the nHA/MAO coatings was higher than that of μHA/MAO coatings and magnesium alloy after cultured for 24 h(*$P < 0.05$,compared to μHA/MAO coatings and magnesium alloy); (c): Fluorescence micrographs of the osteoblast cells cultured for 24 h on nHA/MAO coatings, μHA/MAO coatings and magnesium alloy. Living cells (green) and dead cells (red) were stained with acridine orange/ethidium bromide and were visualized using fluorescence microscopy; (d): Staining of IGF-1 of cells cultured on three samples

Graphic of abstract

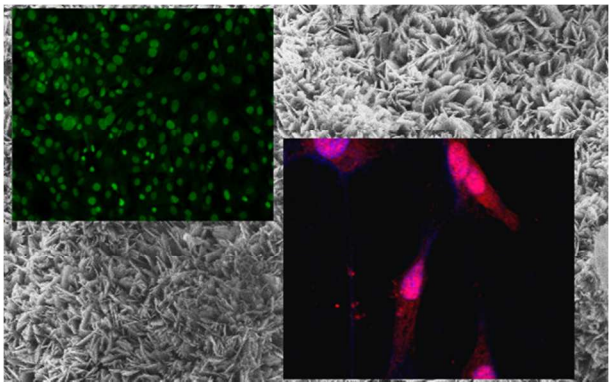

Fabrication and biocompatibility investigation of hydroxyapatite coatings electrelectrodeposites on micro-arc oxidized magnesium alloys via static magnetic.